

# Neutron star universal relations with microscopic equations of state

**J.-B. Wei<sup>1</sup>, A. Figura<sup>1</sup>, G. F. Burgio<sup>1</sup>, H. Chen<sup>2</sup> and H.-J. Schulze<sup>1</sup>**

<sup>1</sup> INFN Sezione di Catania and Dipartimento di Fisica, Università di Catania, Via Santa Sofia 64, 95123 Catania, Italy

<sup>2</sup> School of Mathematics and Physics, China University of Geosciences, Lumo Road 388, 430074 Wuhan, P.R. China

September 2018

**Abstract.** We calculate neutron star's moment of inertia and deformabilities using various microscopic equations of state for nuclear and hybrid star configurations. We confirm several universal relations between the various observables in these cases. We focus in particular on the constraints for the neutron star radii imposed by a determination of the average tidal deformability of the binary neutron star system GW170817. We find compatible radii between 12 and 13 kilometers and identify the suitable equations of state.

*Keywords:* neutron star, equation of state, universal relations

Submitted to: *J. Phys. G: Nucl. Part. Phys.*

## 1. Introduction

Neutron star (NS) observations allow us to probe the equation of state (EOS) of nuclear matter [1, 2] well beyond the densities available in terrestrial laboratories. For example, observations of the NS mass–radius relation [3–6] and the mass–moment-of-inertia relation [7] could ideally be used to infer the NS EOS within a certain observational uncertainty. While the masses of several NSs are known with good precision [8], information on their radii is currently scarce and not very accurate [6, 9–12], and direct measurements of the moment of inertia are so far not possible. However, simultaneous measurement of both quantities for several objects is required in order to constrain the EOS of NS matter and allow conclusions regarding the composition of matter under such extreme conditions.

The recent observation of gravitational waves emitted during the merger of two corotating NSs [13] has opened the door to new possibilities of obtaining information on the structural properties of these objects, most prominently their masses and radii. Binary NSs are, in fact, one of the most promising GW sources [14, 15] for ground-based, second-generation detectors, such as Advanced LIGO [16] and Advanced VIRGO [17].

Comparing the observed GW signal with theoretical simulations, some NS observables have been identified as easily constrainable by a wave-form analysis. Apart from the chirp

mass [18]  $M_c = (M_1 M_2)^{3/5} / (M_1 + M_2)^{1/5}$  of the binary NS system, in particular the tidal deformability [19, 20]  $\lambda \equiv Q_{ij}/E_{ij}$ , which measures the linear response of the quadrupole deformation  $Q_{ij}$  to a (weak) external gravitational field  $E_{ij}$ , could be well constrained by the new data. In fact upper [13] and lower [21] limits on the dimensionless quantity  $\Lambda \equiv \lambda/M^5$  have been deduced. It is therefore of interest to examine these quantities and their relations with other observables in theoretical calculations of the EOS, and numerous studies have already been performed in this sense [3–5, 21–23].

Also our current work follows this motivation and we provide in this article the results obtained with several ‘microscopic’ EOSs, i.e., those based on many-body calculations employing fundamental free interactions. Microscopic EOSs are complementary to phenomenological EOSs with parameters fitted to properties of nuclear matter and finite nuclei around saturation density, and extrapolated to high density relevant for NSs [24]. Relativistic-mean-field (RMF) models are usually used for this purpose (see, e.g., the recent [21, 25–28] in the present context) and offer by their nature more flexibility but less predictive power than microscopic models.

We examine in particular several EOSs [29] obtained within the Brueckner-Hartree-Fock (BHF) approach to nuclear matter [30–32], and compare with the often-used results of the variational calculation (APR) [33, 34] and the Dirac-BHF method (DBHF) [35–37]. Two phenomenological RMF EOSs are also included for comparison: LS220 [38] and SFHo [39], because they were recently used in an analysis of and shown to be compatible with the GW170817/AT2017gfo event [21, 40]. Furthermore we also examine exotic variants containing hyperons [41–45], as well as hybrid stars obtained by allowing a Gibbs phase transition to quark matter (QM) at high density. We model the quark phase in the Dyson-Schwinger (DS) model [44–49], and construct the phase transition to each of the nucleonic BHF models, thus yielding several different hybrid EOSs detailed later.

We briefly comment that attempts to compute the nuclear EOS in chiral perturbation theory [50, 51], which has the theoretical advantage that two-body and three-body forces are determined in a consistent way, are still severely restricted by the perturbative low-density nature of this approach. Currently reliable results are limited to little more than normal nuclear density, at which point the regularization dependence becomes critical, see, e.g., [52, 53] for some recent illustrative results.

As stated before, a stringent constraint on the EOS via the mass-radius relation would be the measurement of both mass and radius of the same object [3–6]. However, observations of NS radii are indirect and the determination of the radius is affected by several uncertainties (e.g., composition of the atmosphere, distance of the source, magnetic field; see, e.g., [54–57]). Therefore precise estimations of NS radii are very difficult because more model dependent than those of masses. Currently, the most reliable constraints can be inferred from observations of quiescent low-mass X-ray binaries (qLMXBs) in globular clusters [9, 58, 59], because their atmospheres can be reliably modelled and their distances can be accurately determined. Constraints can also come from observations of type-I X-ray bursts [3–5], but this kind of analysis is still a matter of debate [8, 9, 60–62]. Further information on radii could also be inferred from X-ray pulsation in millisecond pulsars [63]. Future high-precision telescopes

and missions like NICER [64–66], ATHENA+ [67, 68], and SKA [69, 70] are expected to improve our knowledge on the NS mass-radius relation.

This paper is organized as follows. In Sec. II we give a brief overview of the hadronic and hybrid EOSs we are using. In Sec. III we specify some technical details regarding the computation of moment of inertia and tidal deformability. The numerical results obtained for those quantities along with the mass-radius relation are presented in Sec. IV for the different EOSs, where we also investigate correlations with  $M$  and  $R$  and scrutinize various universality relations. Sec. V contains the conclusions.

## 2. Equations of state

In this section we will briefly discuss the EOSs used in this paper, which are mainly microscopic EOSs based on many-body calculations. For nuclear (hadronic) matter we resort to the BHF many-body theory with realistic two-body and three-body nucleonic forces, which has been extensively discussed in Refs. [30–32]. In particular we examine several EOSs [29] which are based on different nucleon-nucleon potentials, the Argonne  $V_{18}$  [71], the Bonn B (BOB) [72, 73], and the Nijmegen 93 (N93) [74, 75], and compatible three-nucleon forces as input. More precisely, the BOB and N93 are supplemented with microscopic TBF employing the same meson-exchange parameters as the two-body potentials [76–78], whereas  $V_{18}$  is combined either with a microscopic or a phenomenological TBF, the latter consisting of an attractive term due to two-pion exchange with excitation of an intermediate  $\Delta$  resonance, and a repulsive phenomenological central term [79–82]. They are labelled as V18 and UIX, respectively, throughout the paper and in all figures.

The BHF theory has also been extended with the inclusion of hyperons, which might appear in the core of a NS. The hyperonic EOS in this theory turns out to be very soft, and this results in too low NS maximum masses [41–45],  $M < 1.7M_{\odot}$  ( $M_{\odot} \approx 2 \times 10^{33}$ g), well below the current observational limit of about two solar masses [83–85]. Nevertheless, such EOS could be realized in the so-called two-families scenario in which the heaviest stars are interpreted as quark stars, whereas the lighter and smaller stars are hadronic stars [25, 86–89]. We consider two BHF EOSs containing hyperons, which will be labelled as BOB(NN+NY) [41, 42, 44, 45] and V18(NN+NY+YY) [43].

For completeness, we also compare with the often-used results of the Dirac-BHF method (DBHF) [35–37], which employs the Bonn A potential, and the APR EOS based on the variational method [33, 34] and the  $V_{18}$  potential. The LS220 [38] and SFHo [39] phenomenological RMF EOSs are also used for comparison.

As far as the hybrid-star EOS is concerned, it is widely known that the EOS for QM remains uncertain. Whereas the microscopic theory of the nucleonic EOS has reached a high degree of sophistication, the QM EOS is poorly known at zero temperature and at the high baryonic density appropriate for NSs, because it is difficult to perform first-principle calculations of QM. Therefore one can presently only resort to more or less phenomenological models for describing QM, such as the MIT bag model [90] or the Nambu–Jona-Lasinio model [91–93].

The Dyson-Schwinger equations provide a nonperturbative continuum field approach to QCD that can simultaneously address both confinement and dynamical chiral symmetry breaking [94, 95]. In Refs. [44–49] we developed a Dyson-Schwinger model (DSM) for deconfined QM based on this formalism, which was combined with the BHF approach for the hadronic phase in order to model NSs. We describe the quark phase in the DSM with an interaction parameter  $\alpha = 1, 2, 3, 4$  that models the quenching of the free quark-gluon vertex inside QM, see Refs. [44–49] for details. Increasing  $\alpha$  leads to more stable QM in the DSM. We then construct the Gibbs phase transition to each of the nucleonic models. This yields 16 different EOSs (BOB, V18, UIX, N93)  $\otimes$  (DS1, DS2, DS3, DS4), which differ essentially by their onset density of the QM phase and the associated NS maximum mass, both decreasing with increasing  $\alpha$ , i.e., increasingly bound QM.

Properties of the various NS configurations constructed with the considered EOSs are listed in Table 1, i.e., the value of the maximum mass, the corresponding radius, the radius of the  $1.4M_{\odot}$  configuration and its tidal deformability  $\Lambda_{1.4}$ , which will be extensively discussed in Sect. IV. We mention that for the calculation of stellar structure we used the EOSs of Refs. [96, 97] for the outer crust and [98] for the inner crust. The choice of the crust model can influence the radius predictions to a small extent, of the order of 1% for  $R_{1.4}$  [99–101], which is negligible for our purpose. As far as the hybrid stars are concerned, it is an important feature of the DSM that the hybrid star maximum mass decreases with increasing QM fraction [44, 45], and therefore in the following we will consider only BOB+DS1, BOB+DS2, V18+DS1, and N93+DS1, since only for those cases the static maximum mass is larger than 2 solar masses.

### 3. Universal relations and global observables

It is a major purpose of this work to confront the NS observables and their relations obtained with several microscopic EOSs listed in Table 1 to known universality relations. Such universal (EOS-independent) relations between the NS moment of inertia  $I$ , the NS Love number  $k_2$ , and the (spin-induced) NS quadrupole moment  $Q$  (I-Love-Q relations) are discussed in Refs. [22, 23]. Physically, the moment of inertia quantifies how fast a NS can spin for a fixed angular momentum, the quadrupole moment describes how much a NS is deformed away from sphericity, and the Love number characterizes how easy it is to deform a NS. These quantities can be computed by numerically solving for the interior and exterior gravitational field of a NS in a slow-rotation [19] and a small-tidal-deformation approximation [102–104]. Although the moment of inertia is a first-order-in-spin quantity, the quadrupole moment is generated by quadratic spin terms. The tidal Love number [27, 105, 106] is defined by the ratio between the tidally-induced quadrupole moment and the tidal field due to a companion NS, which can be calculated in a similar fashion.

One would expect that all of these quantities should depend quite sensitively on the NS EOS; instead they seem to satisfy almost universal relations when plotted against each other in the proper way. Possible explanations for this phenomenon are reviewed in chapter 5 of [23], but an ultimate formal proof is currently still missing. Universal relations have various useful

**Table 1.** Properties of NSs listed according to the considered EOSs. See text for details.

EOS	$M_{\max}$ [ $M_{\odot}$ ]	$R_{M_{\max}}$ [km]	$R_{1.4}$ [km]	$\Lambda_{1.4}$	Type	Ref.
BOB	2.51	11.32	12.85	584	nucleonic	[29]
BOB+DS1	2.30	12.13	12.85	584	hybrid	[44]
BOB+DS2	2.02	11.95	12.85	584	hybrid	[44]
BOB+DS3	1.79	11.72	12.75	539	hybrid	[44]
BOB+DS4	1.60	11.38	12.12	346	hybrid	[44]
V18	2.34	10.63	12.33	419	nucleonic	[29]
V18+DS1	2.16	11.34	12.33	419	hybrid	[44]
V18+DS2	1.93	11.15	12.33	419	hybrid	[44]
V18+DS3	1.75	10.95	11.96	320	hybrid	[44]
V18+DS4	1.61	10.74	11.36	215	hybrid	[44]
N93	2.13	10.49	12.68	474	nucleonic	[29]
N93+DS1	2.00	11.17	12.68	474	hybrid	[44]
N93+DS2	1.80	10.76	12.64	459	hybrid	[44]
N93+DS3	1.67	10.48	11.76	250	hybrid	[44]
N93+DS4	1.58	10.31	11.05	162	hybrid	[44]
UIX	2.04	10.02	12.03	340	nucleonic	[82]
UIX+DS1	1.98	10.59	12.03	340	hybrid	[44]
UIX+DS2	1.82	10.63	12.03	340	hybrid	[44]
UIX+DS3	1.69	10.44	11.81	10	hybrid	[44]
UIX+DS4	1.59	10.30	11.22	6	hybrid	[44]
APR	2.20	9.92	11.59	274	nucleonic	[33]
DBHF	2.31	11.29	13.10	681	nucleonic	[37]
LS220	2.04	10.67	12.94	542	nucleonic	[38]
SFHO	2.06	10.31	11.93	334	nucleonic	[39]
V18(N+Y)	1.65	9.00	11.92	302	hyperonic	[43]
BOB(N+Y)	1.37	11.07	–	–	hyperonic	[44]

applications in astrophysics, because the measurement of any member of the I-Love-Q trio automatically gives the remaining two quantities without having to know the EOS. The tidal Love number, for example, has been constrained by Advanced LIGO and Advanced Virgo [13], and by combining these results with the I-Love-Q relations, one could equally constrain the moment of inertia and the quadrupole moment of NSs in a binary system, which would also be difficult to measure from GW observations.

In the following we briefly recall the formalism, introducing the compactness parameter  $\beta = GM/Rc^2$ , with  $G$  the gravitational constant and  $c$  the speed of light. Moreover we use geometrized units  $G = c = 1$ .

The moment of inertia  $I = J/\Omega$ ,  $J$  being the angular momentum, and  $\Omega \equiv 2\pi f$  the angular frequency measured by a distant observer (pulsar frequency), the dimensionless ratio

$$\frac{I}{MR^2} = \frac{1}{2\beta} \frac{w_R}{3 + w_R}, \quad w_R = \left. \frac{r}{\omega} \frac{d\omega}{dr} \right|_{r=R} \quad (1)$$

[ $w_R$  involving the metric function  $\omega$ , Eq. (22), is obtained after integrating Eq. (6)] and the

tidal deformability (quadrupole polarizability)  $\lambda$ ,  $\Lambda \equiv \lambda/M^5$ , or equivalently the tidal Love number  $k_2$  [19, 27, 102–106],

$$k_2 = \frac{3}{2} \frac{\lambda}{R^5} = \frac{3}{2} \beta^5 \Lambda \quad (2)$$

$$= \frac{8}{5} \frac{\beta^5 z}{6\beta(2-y_R) + 6\beta^2(5y_R-8) + 4\beta^3(13-11y_R) + 4\beta^4(3y_R-2) + 8\beta^5(1+y_R) + 3z \ln(1-2\beta)}, \quad (3)$$

$$z \equiv (1-2\beta^2)[2-y_R+2\beta(y_R-1)],$$

can be calculated in general relativity together with the TOV equations for pressure  $p$  and enclosed mass  $m$  of a static NS. We follow the method outlined in Refs. [2, 27], namely solve the system of four coupled first-order differential equations,

$$\frac{dp}{dr} = -\frac{m\varepsilon(1+p/\varepsilon)(1+4\pi r^3 p/m)}{r^2(1-2m/r)}, \quad (4)$$

$$\frac{dm}{dr} = 4\pi r^2 \varepsilon, \quad (5)$$

$$\frac{dw}{dr} = \frac{4\pi r(\varepsilon+p)(4+w)}{1-2m/r} - \frac{w(3+w)}{r}, \quad (6)$$

$$\frac{dy}{dr} = -\frac{y^2}{r} - \frac{y-6}{r-2m} - rQ,$$

$$Q \equiv 4\pi \frac{(5-y)\varepsilon + (9+y)p + (\varepsilon+p)/c_s^2}{1-2m/r} - \left[ \frac{2(m+4\pi r^3 p)}{r(r-2m)} \right]^2, \quad (7)$$

with the EOS  $\varepsilon(p)$  as input and  $c_s^2 = d\varepsilon/dp$ . The initial values are

$$[p, m, w, y](r=0) = [p_c, 0, 0, 2] \quad (8)$$

and  $w_R \equiv w(R)$ ,  $y_R \equiv y(R)$ . In the case of an energy density discontinuity  $\delta\varepsilon$  in the EOS (hybrid stars with Maxwell construction or pure quark stars without crust), a separate finite contribution

$$y_c = -3\delta\varepsilon/\bar{\varepsilon} \quad (9)$$

has to be added to  $y$  during the integration, see Refs. [3–5]. The results have been compared with the output of the RNS code [107] in the limit of vanishing rotation frequency, and excellent agreement has been found.

In the case of an asymmetric binary system,  $(M, R)_1 + (M, R)_2$ , with mass asymmetry  $q = M_2/M_1$ , and known chirp mass

$$M_c = \frac{(M_1 M_2)^{3/5}}{(M_1 + M_2)^{1/5}}, \quad (10)$$

the effective deformability is given by

$$\tilde{\Lambda} = \frac{16(1+12q)\Lambda_1 + (q+12)\Lambda_2}{13(1+q)^5} \quad (11)$$

with

$$\frac{[M_1, M_2]}{M_c} = \frac{297}{250} (1+q)^{1/5} [q^{-3/5}, q^{2/5}]. \quad (12)$$

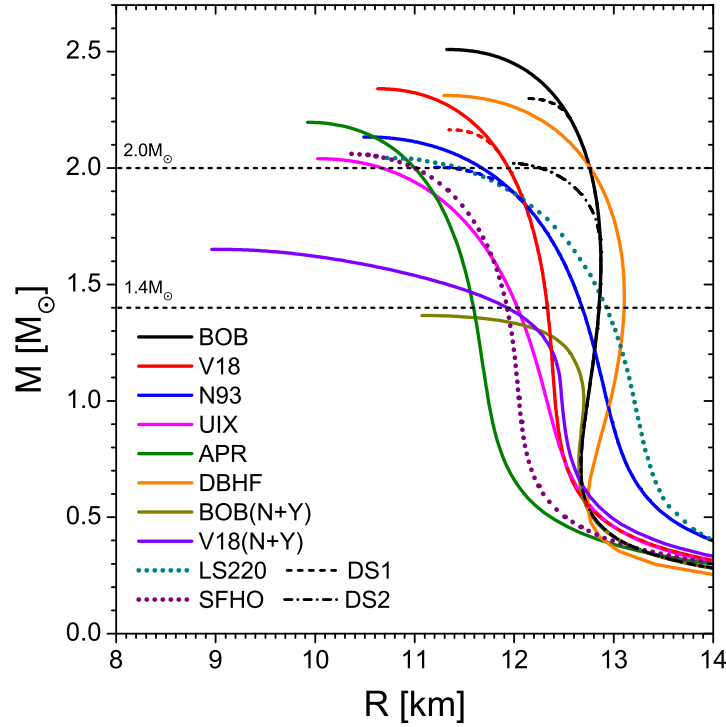


**Figure 1.** Mass-radius relations for different EOSs. Solid (dotted) curves are plotted for microscopic (phenomenological) EOSs. Dashed and dot-dashed lines indicate hybrid stars in the DSM approach, see text.

The analysis of the GW170817 event [13] provided the data  $M_c/M_\odot = 1.188^{+0.004}_{-0.002}$  [corresponding to  $M_1 = M_2 = 1.365 M_\odot$  for a symmetric binary system],  $q = M_2/M_1 = 0.7 - 1$  [corresponding to maximum asymmetry  $(M_1, M_2) = (1.64, 1.15) M_\odot$ ], and  $\tilde{\Lambda} < 800$  from the phase-shift analysis of the observed signal. The limit on  $\tilde{\Lambda}$  was recently updated to  $70 < \tilde{\Lambda} < 720$  [108], but we will keep using the original limit in this work.

## 4. Results and discussion

### 4.1. Mass-radius relations

Let us start by discussing the mass-radius relations of the different EOSs we consider. They are shown in Fig. 1, where results obtained with microscopic (phenomenological) EOSs are displayed as solid (dotted) lines. Moreover we consider the four EOSs for hybrid stars with  $M_{\max} > 2M_\odot$  in Table 1, obtained by performing a Gibbs phase transition between the BOB, V18, or N93 hadronic EOS and the DSM QM EOS characterized by two different values of  $\alpha = 1, 2$  (DS1, DS2). They are displayed as dashed and dot-dashed lines, respectively. We observe that most models give values of the maximum mass larger than  $2M_\odot$ , and therefore are compatible with current observational data [83–85]. However, the two hyperonic EOSs do not fulfill the observational limit. We nevertheless include them in our analysis in order to see whether they reveal irregular features elsewhere. Some recent analyses of the GW170817

event indicate an upper limit of the maximum mass of about  $2.2M_{\odot}$  [40, 109, 110], with which several of the microscopic EOSs would be compatible.

According to Fig. 1 (see also Table 1), the predicted radii for a  $M = 1.4M_{\odot}$  NS span a range ( $11.6 \lesssim R_{1.4} \lesssim 13.2$ ) km. Those values are in agreement with the ones reported in Ref. [111], where an analysis of the results of GW170817 was performed by using a general polytropic parametrization of the EOS compatible with perturbative QCD at very high density. In Ref. [111] it has been shown that the tidal deformability limit of a  $1.4M_{\odot}$  NS,  $\Lambda_{1.4} < 800$ , as found in GW170817, implies a radius  $R_{1.4} < 13.6$  km. Quite similar upper limits have been obtained in [112–114].

Interpretation of the GW170817 event also allowed to establish *lower* limits on the NS radius: The condition of (meta)stability of the produced hypermassive star after merger allowed to exclude very soft EOSs [40] and to set thus a lower limit on the radius,  $R_{1.6} > 10.7$  km [115], confirmed by similar recent analyses [112, 113] in which  $R_{1.4} > (11.5 - 12)$  km. An even higher lower limit  $R_{1.4} > 12.55$  km [116] has been deduced from the measurement of the neutron skin of  $^{208}\text{Pb}$  in the PREX experiment [117]. Simulations with several different EOSs set also a lower limit on the effective deformability Eq. (11),  $\tilde{\Lambda} > 400$  [21], related to the black hole formation time and the accretion disk mass of material left out of the black hole. The latter was constrained from optical/infrared observations of the remnant AT2017gfo [118–122]. Small values of  $\tilde{\Lambda}$  and therefore small values of  $R$  imply very fast black hole formation and little material left in the disk, which is incompatible with observation. A correlated lower limit  $R_{1.4} \gtrsim 12$  km is obtained in this way.

On the other hand, smaller radii than these lower limits were deduced from observations of thermal emission from accreting NSs in quiescent LMXBs. In fact, by analyzing their X-ray spectra, the observations seem to suggest for stars of mass about  $(1.4 - 1.5)M_{\odot}$  a radius in the range  $(9.9 - 11.2)$  km [6]. Those results have been criticized in [3–5]: in particular the estimates of the radii are affected by the uncertainties on the composition of the atmosphere. If the atmosphere contains He, significantly larger radii are extracted. More recently [12] it was shown that when allowing for the occurrence of a first-order phase transition in dense matter (Model C),  $R_{1.4}$  is smaller than 12 km to 95% confidence. However,  $R_{1.4}$  could be larger if NSs have uneven temperature distributions. Clearly, no firm conclusions can yet be reached and we need to wait for new data such as the ones collected by the NICER mission, in order to obtain independent and precise information on NS radii.

We remark that this clash between large radii from GW170817 and small radii from quiescent LMXBs (if confirmed) could be resolved in the two-families or twin-star scenarios, in which small and big stars of the same mass could coexist as hadronic and QM stars [25, 86–89].

#### 4.2. The moment of inertia $I$

Taking for granted the validity of a universality relation, the moment of inertia  $I$  of a NS can be expressed as a function of the NS mass and radius, and therefore the radius could be determined if the mass and the moment of inertia of the NS is known [7, 123]. Dimensionally,



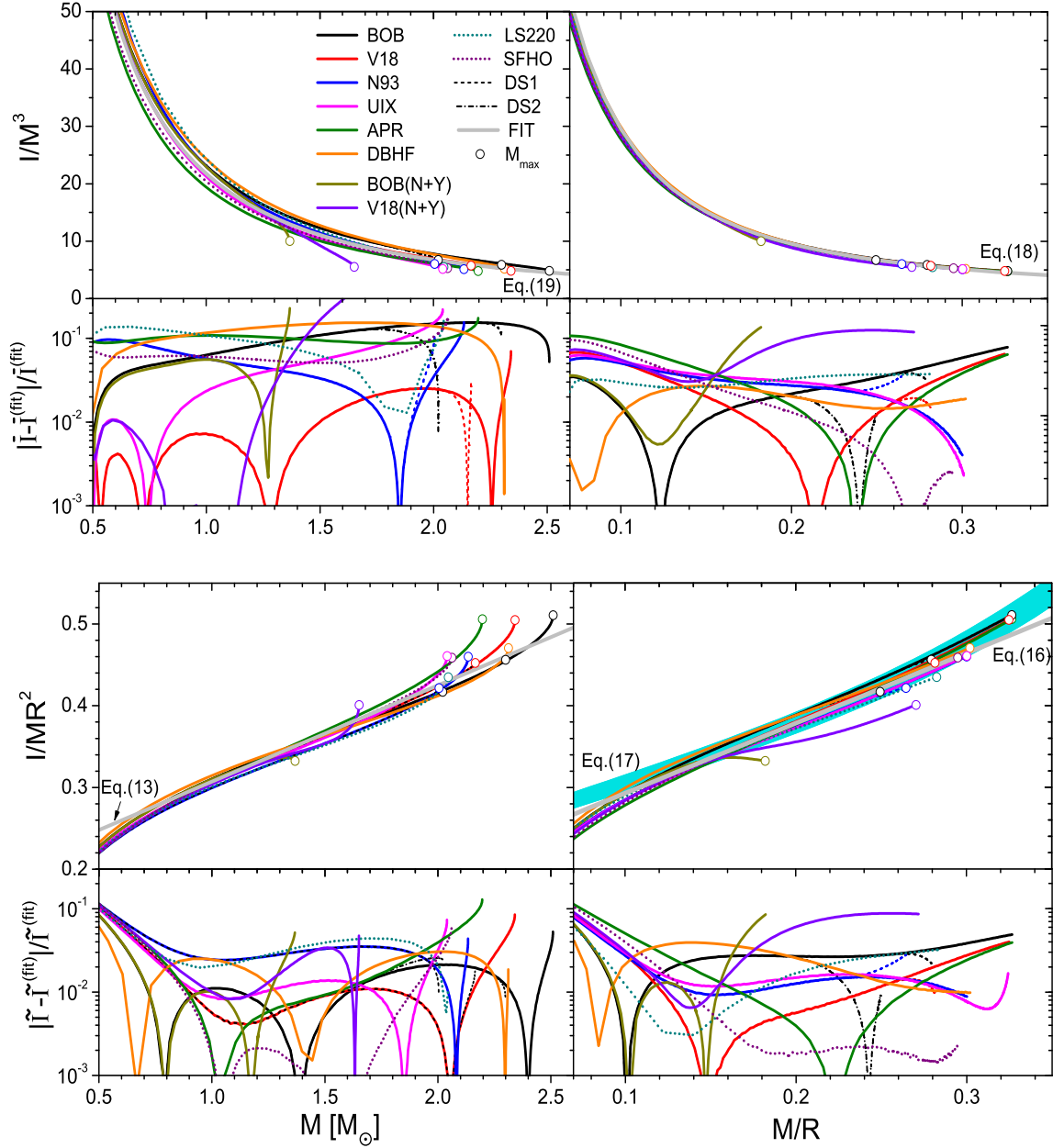


**Figure 2.**  $I/MR^2$  (lower panels) and  $I/M^3$  (upper panels) vs.  $M$  (left panels) and  $M/R$  (right panels) for the 10+4 different nucleonic+hybrid EOSs shown in Fig. 1. Configurations of  $M = M_{\max}$  are indicated by markers. The grey curves indicate the fits according to Eqs. (13),(16),(18),(19). The fit Eq. (17) taken from Refs. [3–5] is shown for comparison as a blue band, see text. In each panel, the upper part shows the results for the different EOSs, and the lower part the fractional deviations from the grey fit curves.

the moment of inertia is proportional to the star’s mass times its radius squared, so a measurement of the moment of inertia to a given accuracy provides approximately twice that accuracy for a radius identification. As already stated in Ref. [7], estimating a NS moment of inertia from timing observations of a binary radio pulsar has significant implications for constraining the EOS. In some respect, a measurement of the moment of inertia could be

more useful than a radius measurement of the same accuracy. However, the moment of inertia of a rotating NS has not yet been measured directly.

In Fig. 2 we show the moment of inertia normalized in two different ways,  $I/MR^2$  (lower panels) and  $I/M^3$  (upper panels) vs. the gravitational mass  $M$  (left panels) and the compactness  $\beta$  (right panels), for the same EOSs as shown in Fig. 1.

We observe in general that all curves lie within ‘‘universality bands,’’ i.e., they are nearly EOS independent. For example, the universal relation in the  $I/MR^2$  vs.  $M$  plot, indicated by a grey curve, is quantified as a simple linear fit, valid in the interval  $1 < M/M_\odot < 2$ ,

$$\frac{I}{MR^2} \approx 0.189 + 0.118 \frac{M}{M_\odot} \pm 0.016. \quad (13)$$

For fixed (measured)  $M$  and  $I$  and unknown  $R$  we have then

$$\delta(f \equiv \frac{I}{MR^2}) = -\frac{2I}{MR^3} \delta R = -2f \frac{\delta R}{R} \quad (14)$$

and thus the universality band determines  $R$  with accuracy

$$\frac{\delta R}{R} = \frac{1}{2} \frac{\delta f}{f} \approx \frac{0.016}{0.4} \lesssim 4\%. \quad (15)$$

For the  $I/MR^2$  vs.  $M/R$  plot, the equivalent fit for our chosen set of microscopic EOSs reads (grey curve)

$$\frac{I}{MR^2} \equiv 0.207 + 0.857\beta \pm 0.011, \quad (16)$$

to be compared with the one reported in Ref. [3–5], obtained with a larger set of EOSs, displayed as a blue band,

$$\frac{I}{MR^2} \approx (0.237 \pm 0.008)(1 + 2.844\beta + 18.91\beta^4) \quad (17)$$

It may be noted that the fit vs.  $M$  fails mainly for large masses  $M > 2M_\odot$ , whereas the fit vs.  $\beta$  fails for hyperonic stars with low  $M_{\max}$ . The latter feature is caused by the small radius of the maximum mass configuration for the hyperonic EOSs, see Fig. 1, which leads to an ‘abnormaly’ large value of  $\beta = M/R$  close to the (small) maximum mass. Turning the universality argument around, future simultaneous measurement of  $M, R, I$  could therefore provide evidence for the presence of hyperons in a NS, at least close to the maximum mass configuration.

The upper panels of Fig. 2 show the results obtained for the quantity  $I/M^3$  as advocated in [124], together with the fits

$$\frac{I}{M^3} \equiv 0.8134\beta^{-1} + 0.2101\beta^{-2} + 0.003175\beta^{-3} - 0.0002717\beta^{-4} \quad (18)$$

obtained in [124] and

$$\frac{I}{M^3} \equiv 1.0334M^{-1} + 30.7271M^{-2} - 12.8839M^{-3} + 2.8841M^{-4} \quad (19)$$

obtained by us. Summarizing, in all four panels (except the case of  $I/M^3$  vs.  $M$  plot), the deviations of the individual EOSs from the universal fits are of the order of a few percent, largest with the hyperonic EOSs.

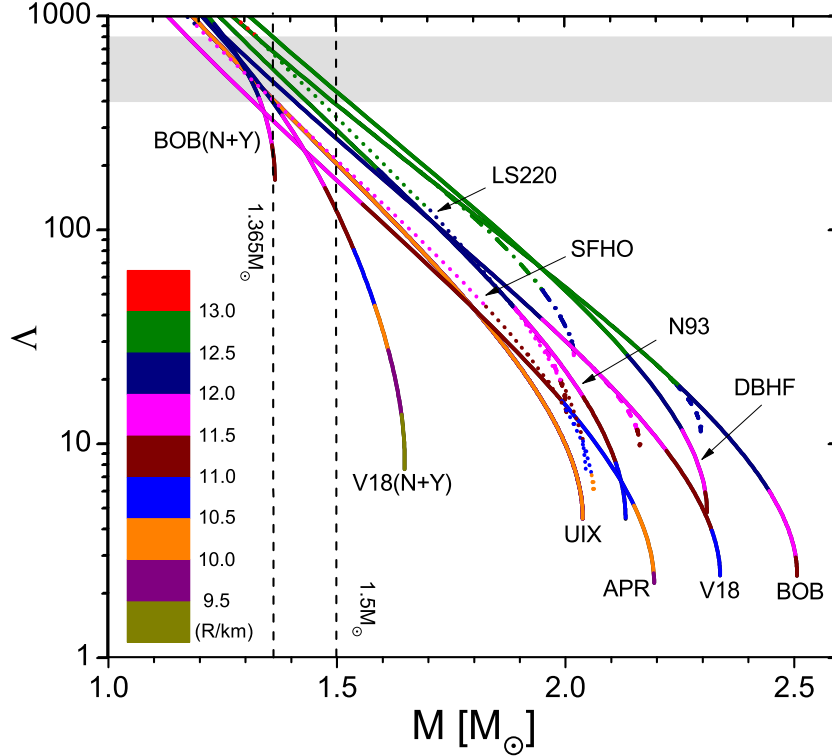


**Figure 3.** Correlations between  $M$ ,  $R$ , and  $\Lambda$  for a single NS with different EOSs, see Fig. 1. Dashed and dot-dashed curves display hybrid stars with DS1 and DS2, respectively. The shaded area is constrained by the interpretation of the GW170817 event as a symmetric NS merger.

#### 4.3. The tidal deformability $\Lambda$

We now turn to discuss a further important global observable, the tidal deformability  $\Lambda$  of a single NS, see Eq. (3). Fig. 3 shows  $\Lambda$  as a function of  $M$  and  $R$  for the various EOSs considered in this paper. The information on the radius  $R$  is encoded in the colored segments of the curves. The grey band represents the observational limits derived in Refs. [13, 21] mentioned before,  $400 < \Lambda < 800$ , deduced from a multimessenger analysis of the GW170817 event on the amplitude of tidal effects during the binary inspiral, combined with an analysis of the UV/optical/infrared counterpart with kilonova models. The black dashed line at fixed mass  $M = 1.365 M_\odot$  indicates the masses of each NS for a symmetric binary system in GW170817, whereas the line located at  $1.5 M_\odot$  represents the constraint derived in Ref. [111].

One notes that the conditions  $M = 1.365 M_\odot$  and  $400 < \Lambda < 800$  imply  $12 \text{ km} \lesssim R \lesssim 13 \text{ km}$ , with the compatible EOSs V18(N+Y), UIB, V18, N93, BOB, DBHF in order of increasing radius (see also Table 1). Also the phenomenological EOS labelled LS220 fulfills the constraint, as well as trivially the hybrid stars constructed with DS1 and DS2 EOSs, which at  $M = 1.365 M_\odot$  are still purely nucleonic. On the other hand, APR, BOB(N+Y), and SFHO (marginally) do not fulfill the  $\Lambda > 400$  constraint.

The same kind of information can be derived also by displaying the tidal deformability  $\Lambda$  of a single NS as a function of the radius  $R$  and the compactness  $\beta$  for the considered EOS,

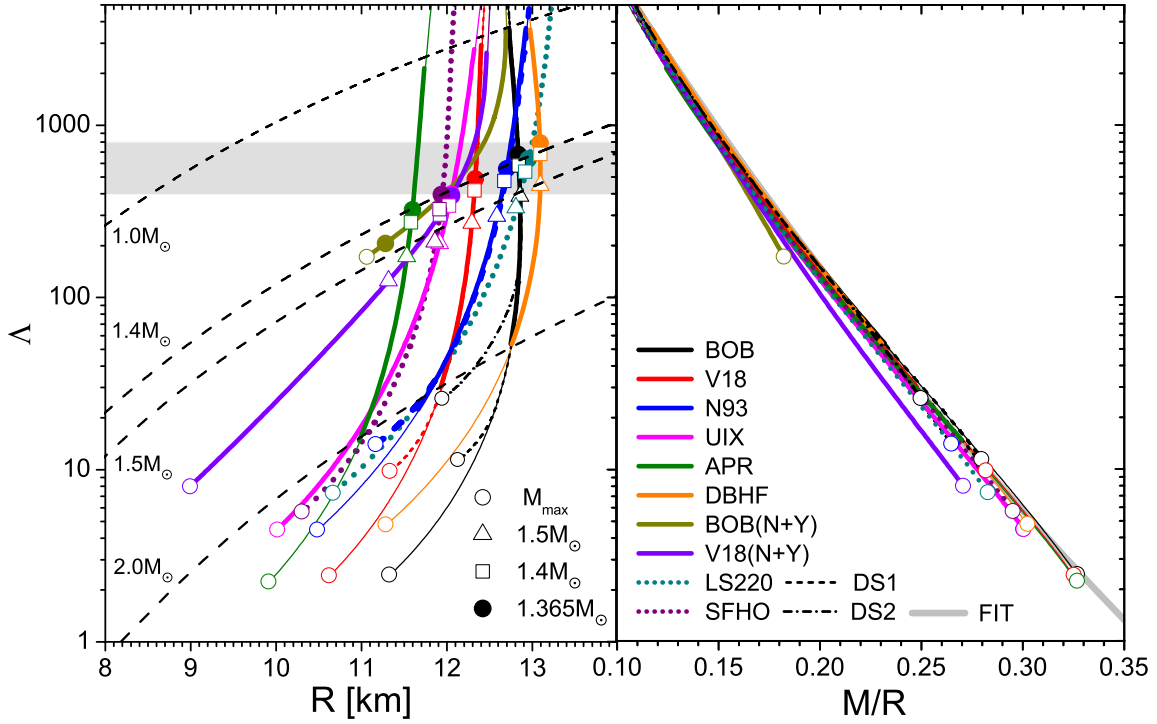


**Figure 4.** Correlations between  $\Lambda, M, R$  for a single NS with different EOSs. The shaded area is constrained by the interpretation of the GW170817 event as a symmetric NS merger. The dashed (left panel) or grey (right panel) curves show the predictions according to the universal fit Eq. (20).

and this is shown in Fig. 4. As before, the grey band represents the constraints discussed above, and the different curves are obtained for the different EOSs. The curves have a bold width in the interval  $1 < M/M_\odot < 2$ . The full circles represent the  $(\Lambda, R)$  configurations at  $M = 1.365 M_\odot$ , whereas the open squares and triangles indicate  $M = 1.4 M_\odot$  and  $M = 1.5 M_\odot$  configurations, respectively. The endpoints, displayed as open circles, represent the maximum mass for that chosen EOS.

A universal relation of the individual tidal deformabilities of NSs as function of the stellar compactness was introduced in Ref. [22], and in Ref. [23] the following fit was proposed

$$\beta = 0.36 - 0.0355 \ln \Lambda + 0.000705 (\ln \Lambda)^2, \quad (20)$$

which holds to within 6.5% for a large set of NS EOSs [23]. The dashed black lines in the left panel and the solid grey line in the right panel represent the results of Eq. (20), and particularly in the right panel one can observe that the fit works well (slightly overestimating the values of  $\Lambda$ ) also for our set of microscopic EOSs, except for the very soft ones including hyperons.

For completeness we confirm also the extremely tight universal relation between the dimensionless quantities  $\bar{I} \equiv I/M^3$  and  $\Lambda$  [23], namely

$$\begin{aligned} \ln(I/M^3) = & 1.496 + 0.05951 \ln \Lambda + 0.02238 (\ln \Lambda)^2 \\ & - 6.953 \times 10^{-4} (\ln \Lambda)^3 + 8.345 \times 10^{-6} (\ln \Lambda)^4. \end{aligned} \quad (21)$$

The comparison with our EOSs is shown in Fig. 5 (left plot) and confirms the validity of

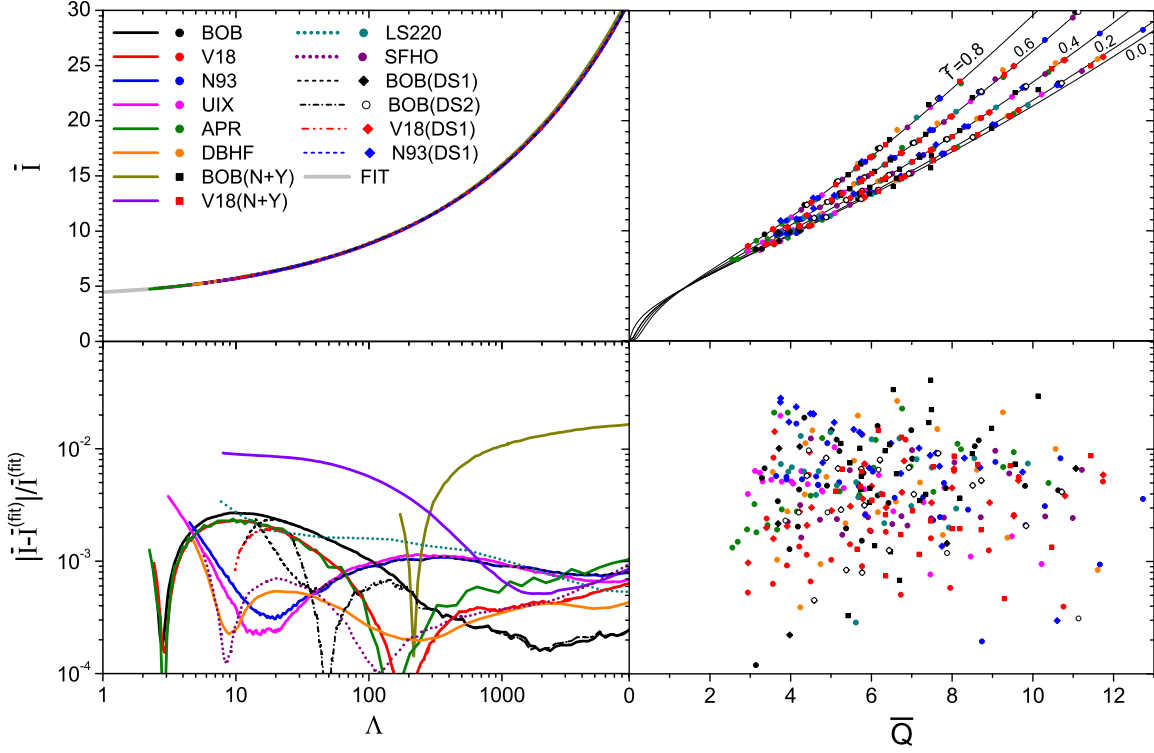


**Figure 5.** Relation between dimensionless quantities  $\bar{I} = I/M^3$  and  $\Lambda$  (left plot) or  $\bar{Q} = -QM/(I\Omega)^2$  (right plot) in comparison with the fits Eq. (21) or Eqs. (26,27) (curves), respectively. The colored markers in the right plot show results obtained with different EOSs at fixed rotation parameter  $\tilde{f} \equiv 20Rf = 0.0, 0.2, 0.4, 0.6, 0.8$ . In the bottom panels, relative errors between the fitting curves and numerical results are displayed.

the fit (grey curve). The bottom of this figure shows the fractional errors between the fitting function and the numerical results, and they amount to less than 1%, being a bit larger for EOSs including hyperons.

#### 4.4. The quadrupole moment $Q$

A further universal, i.e., EOS-independent, relation involves the moment of inertia  $I$  and the spin-induced quadrupole moment  $Q$ , as proposed in Refs. [22, 23]. This relation was derived in the slow-rotation and small-tidal-deformation approximations, leaving open the question of its general validity, faced in some successive papers [28, 125]. Here, we analyze the validity of this universal relation for our set of microscopic EOSs.

For analyzing the field equations of the rotating NS and compute  $Q$ , we use the RNS code [107], which assumes steady rotation and axisymmetric structure. Therefore the space-time metric can be expressed as [126]

$$ds^2 = -e^{\gamma+\rho} dt^2 + e^{2\beta} (dr^2 + r^2 d\theta^2) + e^{\gamma-\rho} r^2 \sin^2\theta (d\phi - \omega dt)^2, \quad (22)$$

where the potentials  $\gamma, \rho, \beta, \omega$  are functions of  $r$  and  $\theta$  only. The quadrupole moment

calculated using RNS,  $Q^{\text{RNS}}$ , has to be corrected [127–129] and is given by [126, 130]

$$Q = Q^{\text{RNS}} - \frac{4}{3} \left( \frac{1}{4} + b_0 \right) M^3, \quad (23)$$

where  $M$  is the mass of the star, and the parameter  $b_0$  is given by

$$b_0 = - \frac{16\sqrt{2\pi}r_{\text{eq}}^4}{M^2} \int_0^{\frac{1}{2}} \frac{s^3 ds}{(1-s)^5} \int_0^1 d\mu \sqrt{1-\mu^2} P(s, \mu) e^{\gamma+2\beta} T_0^{\frac{1}{2}}(\mu). \quad (24)$$

Here  $r_{\text{eq}}$  is the value of the coordinate radius at the equator,  $s = r/(r+r_{\text{eq}})$  is a compacted radial coordinate,  $\mu = \cos(\theta)$ ,  $P(s, \mu)$  is the pressure, and  $T_0^{\frac{1}{2}}(\mu) = \sqrt{2/\pi} C_0(\mu)$  with  $C_0$  the 0th-order Gegenbauer polynomial.

In order to investigate universal relations, the following dimensionless quantities were introduced [125]

$$\bar{I} \equiv \frac{I}{M^3}, \quad \bar{Q} \equiv - \frac{QM}{(I\Omega)^2}. \quad (25)$$

In Fig. 5 (right plot) we display  $\bar{I}$  vs.  $\bar{Q}$  for the various EOSs and for different normalized rotational frequencies  $\tilde{f} \equiv 20Rf = 0.0, 0.2, 0.4, 0.6, 0.8$ . (The normalization is such that  $f = 1$  kHz corresponds to  $\tilde{f} \approx 1$  for  $R = 15$  km). The  $\tilde{f} = 0.0$  curve is the one of Refs. [22, 23], obtained in the limit of small frequency,

$$\ln \bar{I} = 1.393 + 0.5471 \ln \bar{Q} + 0.03028 (\ln \bar{Q})^2 + 0.01926 (\ln \bar{Q})^3 + 4.434 \times 10^{-4} (\ln \bar{Q})^4. \quad (26)$$

The other curves represent the refined fits given in Ref. [125], where an explicit dependence of the above coefficients on  $\tilde{f}$ , or alternatively on the parameter  $a \equiv I\Omega/M^2$ , was introduced for the range  $0.2 < \tilde{f} < 1.2$ ,  $0.1 < a < 0.6$ ,  $1.5 < \bar{Q} < 15$ :

$$\ln \bar{I} \approx \sum_{i,j=0,4} \mathcal{A}_{ij} a^i (\ln \bar{Q})^j \approx \sum_{i,j=0,4} \mathcal{B}_{ij} \tilde{f}^i (\ln \bar{Q})^j, \quad (27)$$

with the parameters  $\mathcal{A}_{ij}$  and  $\mathcal{B}_{ij}$  to be found in Ref. [125].

One observes that also for our set of EOSs the fit works very well, the relative deviations remaining below three percent in most cases, as shown in the lower panel of Fig. 5 (right). As motivated in Ref. [125], this allows in principle the determination of the NS radius appearing in the definition of  $\tilde{f} = 20Rf$ , if the correlated quantities  $\bar{I}, \bar{Q}$  are sufficiently well known. We notice, however, that the spin-induced quadrupole moment  $Q$  is largely degenerate with the mass ratio and the spins, and this makes it very difficult to measure independently [131].

## 5. Conclusions

We have confirmed the validity of several universal relations among the moment of inertia  $I$ , the tidal deformability  $\Lambda$ , and the quadrupole moment  $Q$ , as proposed some years ago [22, 23]. In particular, we have examined several microscopic EOSs obtained within the BHF approach to nuclear matter, along with the well-known variational APR and the DBHF EOS, and compared with two phenomenological RMF EOSs, LS220 and SFHo. We have also analyzed the BHF EOS for stellar matter containing hyperons, as well as hybrid stars with quark matter at high density, modeled in the Dyson-Schwinger theoretical framework. The

strongest deviations from universality are exhibited by the hyperonic EOSs, with the eventual possibility to identify their presence in NSs in this way.

We have demonstrated that the microscopic equations of state derived some time ago in the BHF formalism and based on meson-exchange nucleon-nucleon potentials and consistent microscopic three-body forces, are fully compatible with new constraints imposed by interpretation of the first observed neutron-star merger event GW170817. In particular, they respect the lower  $2M_{\odot}$  limit of the NS maximum mass and feature typical radii between 12 and 13 km, constrained by tightly correlated values of the tidal deformability  $\Lambda$ . The same holds true also for the relativistic DBHF EOS.

We stress that all results presented here were obtained by assuming that Einstein's general relativity (GR) is the correct theory of gravity. However, NS are also unique probes of strong-field gravitational physics, and therefore extensions of GR have to be taken into account. For any given EOS, theories that modify the strong-field dynamics of GR generally predict static properties, e.g., mass, radius, and moment of inertia, that are different from those in Einstein's theory. The rich literature available on NS treated in modified theories of gravity reveals a high degree of degeneracy in the main properties of relativistic stars [132], and this highlights the potential of future GW measurements to determine the behavior of gravity in the strong-field regime.

The detection of gravitational waves by the LIGO/Virgo collaboration in 2015, and the successive binary neutron star merger event GW170817, opened a new astronomical eye to the Universe, and NSs play a key role in this respect, having the potential of being extremely prolific gravitational wave emitters in terms of expected detection rates. Therefore we are looking forward to more refined constraints to be obtained soon from further merger events and new facilities.

## Acknowledgments

We acknowledge useful discussions with A. Drago and G. Pagliara. H. Chen acknowledges financial support from NSFC (11475149, U1738130), and J.-B. Wei acknowledges the China Scholarship Council (CSC File No. 201706410092) for financial support. Partial support comes also from "PHAROS," COST Action CA16214.

## References

- [1] Lattimer J M and Prakash M 2007 *Phys. Rep.* **442** 109 – 165
- [2] Lattimer J M and Prakash M 2016 *Phys. Rep.* **621** 127–164
- [3] Lattimer J M and Prakash M 2001 *Astrophys. J.* **550** 426
- [4] Steiner A W, Lattimer J M and Brown E F 2010 *Astrophys. J.* **722** 33
- [5] Steiner A W, Lattimer J M and Brown E F 2013 *Astrophys. J. Lett.* **765** L5
- [6] Özel F and Freire P 2016 *Ann. Rev. Astron. Astrophys.* **54** 401–440
- [7] Lattimer J M and Schutz B F 2005 *Astrophys. J.* **629** 979
- [8] Lattimer J M 2012 *Ann. Rev. Nucl. Sci.* **62** 485–515
- [9] Guillot S, Servillat M, Webb N A and Rutledge R E 2013 *Astrophys. J.* **772** 7
- [10] Lattimer J M and Steiner A W 2014 *Astrophys. J.* **784** 123

- [11] Steiner A W, Lattimer J M and Brown E F 2016 *Eur. Phys. J. A* **52** 18
- [12] Steiner A W, Heinke C O, Bogdanov S, Li C K, Ho W C G, Bahramian A and Han S 2018 *Mon. Not. Roy. Astron. Soc.* **476** 421–435
- [13] Abbott B *et al.* (Virgo, LIGO Scientific) 2017 *Phys. Rev. Lett.* **119** 161101
- [14] Faber J A and Rasio F A 2012 *Living Reviews in Relativity* **15** 8
- [15] URL <http://www.advancedligo.mit.edu/>
- [16] URL <https://www.ligo.org/>
- [17] URL <http://public.virgo-gw.eu/the-virgo-collaboration/>
- [18] Peters P C and Mathews J 1963 *Phys. Rev.* **131** 435–439
- [19] Hartle J B 1967 *Astrophys. J.* **150** 1005–1029
- [20] Flanagan E E and Hinderer T 2008 *Phys. Rev. D* **77** 021502
- [21] Radice D, Perego A, Zappa F and Bernuzzi S 2018 *Astrophys. J.* **852** L29
- [22] Yagi K and Yunes N 2013 *Phys. Rev. D* **88** 023009
- [23] Yagi K and Yunes N 2017 *Phys. Rept.* **681** 1–72
- [24] Burgio G F and Fantina A F 2018 arXiv:1804.03020
- [25] Paschalidis V, Yagi K, Alvarez-Castillo D, Blaschke D B and Sedrakian A 2018 *Phys. Rev. D* **97** 084038
- [26] Malik T, Alam N, Fortin M, Providência C, Agrawal B K, Jha T K, Kumar B and Patra S K 2018 *Phys. Rev. C* **98** 035804
- [27] Postnikov S, Prakash M and Lattimer J M 2010 *Phys. Rev. D* **82** 024016
- [28] Doneva D D, Yazadjiev S S, Stergioulas N and Kokkotas K D 2013 *Astrophys. J.* **781** L6
- [29] Li Z H and Schulze H J 2008 *Phys. Rev. C* **78** 028801
- [30] Jeukenne J P, Lejeune A and Mahaux C 1976 *Phys. Rep.* **25** 83–174
- [31] Baldo M 1999 *International Review of Nuclear Physics (World Scientific, Singapore)* **8**
- [32] Baldo M and Burgio G F 2012 *Reports on Progress in Physics* **75** 026301
- [33] Akmal A, Pandharipande V R and Ravenhall D G 1998 *Phys. Rev. C* **58** 1804–1828
- [34] Morales J, Pandharipande V R and Ravenhall D G 2002 *Phys. Rev. C* **66** 054308
- [35] Brockmann R and Machleidt R 1990 *Phys. Rev. C* **42** 1965–1980
- [36] Li G Q, Machleidt R and Brockmann R 1992 *Phys. Rev. C* **45** 2782–2794
- [37] Gross-Boelting T, Fuchs C and Faessler A 1999 *Nucl. Phys. A* **648** 105–137
- [38] Lattimer J M and Swesty F D 1991 *Nucl. Phys. A* **535** 331–376
- [39] Steiner A W, Hempel M and Fischer T 2013 *Astrophys. J.* **774** 17
- [40] Shibata M, Fujibayashi S, Hotokezaka K, Kiuchi K, Kyutoku K, Sekiguchi Y and Tanaka M 2017 *Phys. Rev. D* **96** 123012
- [41] Schulze H J, Polls A, Ramos A and Vidana I 2006 *Phys. Rev. C* **73** 058801
- [42] Schulze H J and Rijken T 2011 *Phys. Rev. C* **84** 035801
- [43] Rijken T A and Schulze H J 2016 *Eur. Phys. J. A* **52** 21
- [44] Chen H, Baldo M, Burgio G F and Schulze H J 2011 *Phys. Rev. D* **84** 105023
- [45] Chen H, Baldo M, Burgio G F and Schulze H J 2012 *Phys. Rev. D* **86** 045006
- [46] Chen H, Wei J B, Baldo M, Burgio G F and Schulze H J 2015 *Phys. Rev. D* **91** 105002
- [47] Chen H, Wei J B and Schulze H J 2016 *Eur. Phys. J. A* **52** 291
- [48] Wei J B, Chen H and Schulze H J 2017 *Chin. Phys. C* **41** 115101
- [49] Wei J B, Chen H, Burgio G F and Schulze H J 2017 *Phys. Rev. D* **96** 043008
- [50] Epelbaum E, Hammer H W and Meißner U G 2009 *Reviews of Modern Physics* **81** 1773–1825
- [51] Machleidt R and Entem D R 2011 *Phys. Rep.* **503** 1–75
- [52] Drischler C, Carbone A, Hebeler K and Schwenk A 2016 *Phys. Rev. C* **94** 054307
- [53] Holt J W and Kaiser N 2017 *Phys. Rev. C* **95** 034326
- [54] Suleimanov V, Poutanen J and Werner K 2011 *Astron. Astrophys.* **527** A139
- [55] Servillat M, Heinke C O, Ho W C G, Grindlay J E, Hong J, van den Berg M and Bogdanov S 2012 *Mon. Not. Roy. Astron. Soc.* **423** 1556
- [56] Potekhin A Y 2014 *Phys. Usp.* **57** 735–770
- [57] Fortin M, Zdunik J L, Haensel P and Bejger M 2015 *Astron. Astrophys.* **576** A68



- [58] Guillot S and Rutledge R E 2014 *Astroph. J. Lett.* **796** L3
- [59] Özel F, Psaltis D, Güver T, Baym G, Heinke C and Guillot S 2016 *Astroph. J.* **820** 28
- [60] Galloway D K and Lampe N 2012 *Astrophys. J.* **747** 75
- [61] Guver T and Özel F 2013 *Astrophys. J.* **765** L1
- [62] Poutanen J, Nättilä J, Kajava J J E, Latvala O M, Galloway D, Kuulkers E and Suleimanov V 2014 *Mon. Not. Roy. Astron. Soc.* **442** 3777–3790
- [63] Bogdanov S 2016 *Eur. Phys. J. A* **52** 37
- [64] URL <https://www.nasa.gov/nicer/>
- [65] Arzoumanian, Z et al 2014 *Proceedings of SPIE* **9144** 914420
- [66] Bogdanov S 2016 *AAS/High Energy Astrophysics Division* **15** 105.05
- [67] URL <http://www.the-athena-x-ray-observatory.eu/>
- [68] Barcons X, Nandra K, Barret D, den Herder J W, Fabian A C, Piro L and Watson M G (Athena Team) 2015 *J. Phys. Conf. Ser.* **610** 012008
- [69] URL <http://skatelescope.org/>
- [70] Watts A et al. 2015 *PoS AASKA* **14** 043
- [71] Wiringa R B, Stoks V G J and Schiavilla R 1995 *Phys. Rev. C* **51** 38–51
- [72] Machleidt R, Holinde K and Elster C 1987 *Phys. Rept.* **149** 1–89
- [73] Machleidt R 1989 *Adv. Nucl. Phys.* **19** 189–376
- [74] Nagels M M, Rijken T A and de Swart J J 1978 *Phys. Rev. D* **17** 768
- [75] Stoks V G J, Klomp R A M, Terheggen C P F and de Swart J J 1994 *Phys. Rev. C* **49** 2950–2962
- [76] Grangé P, Lejeune A, Martzolff M and Mathiot J F 1989 *Phys. Rev. C* **40** 1040–1060
- [77] Zuo W, Lejeune A, Lombardo U and Mathiot J F 2002 *Eur. Phys. J. A* **14** 469–475
- [78] Li Z H, Lombardo U, Schulze H J and Zuo W 2008 *Phys. Rev. C* **77** 034316
- [79] Pudliner B S, Pandharipande V R, Carlson J and Wiringa R B 1995 *Phys. Rev. Lett.* **74** 4396–4399
- [80] Pudliner B S, Pandharipande V R, Carlson J, Pieper S C and Wiringa R B 1997 *Phys. Rev. C* **56** 1720–1750
- [81] Baldo M, Bombaci I and Burgio G F 1997 *A&A* **328** 274–282
- [82] Sharma B K, Centelles M, Viñas X, Baldo M and Burgio G F 2015 *A&A* **584** A103
- [83] Demorest P B, Pennucci T, Ransom S M, Roberts M S and Hessels J W 2010 *Nature* **467** 1081–3
- [84] Fonseca E et al. 2016 *Astrophys. J.* **832** 167
- [85] Antoniadis J et al. 2013 *Science* **340** 6131
- [86] Drago A, Lavagno A, Pagliara G and Pigato D 2016 *Eur. Phys. J. A* **52** 40
- [87] Drago A and Pagliara G 2018 *Astrophys. J.* **852** L32
- [88] Wiktorowicz G, Drago A, Pagliara G and Popov S B 2017 *Astrophys. J.* **846** 163
- [89] Burgio G F, Drago A, Pagliara G, Schulze H J and Wei J B 2018 *Astrophys. J.* **860** 139
- [90] Chodos A, Jaffe R L, Johnson K, Thorn C B and Weisskopf V F 1974 *Phys. Rev. D* **9** 3471–3495
- [91] Buballa M 2005 *Phys. Rept.* **407** 205–376
- [92] Klähn T, Lastowiecki R and Blaschke D B 2013 *Phys. Rev. D* **88** 085001
- [93] Klähn T and Fischer T 2015 *Astrophys. J.* **810** 134
- [94] Roberts C D and Williams A G 1994 *Prog. Part. Nucl. Phys.* **33** 477–575
- [95] Alkofer R and von Smekal L 2001 *Phys. Rept.* **353** 281
- [96] Feynman R P, Metropolis N and Teller E 1949 *Phys. Rev.* **75** 1561–1573
- [97] Baym G, Pethick C and Sutherland P 1971 *Astrophys. J.* **170** 299–317
- [98] Negele J W and Vautherin D 1973 *Nucl. Phys. A* **207** 298–320
- [99] Burgio G F and Schulze H J 2010 *A&A* **518** A17
- [100] Baldo M, Burgio G F, Centelles M, Sharma B K and Viñas X 2014 *Physics of Atomic Nuclei* **77** 1157–1165
- [101] Fortin M, Providência C, Raduta A R, Gulminelli F, Zdunik J L, Haensel P and Bejger M 2016 *Phys. Rev. C* **94**(3) 035804 URL <https://link.aps.org/doi/10.1103/PhysRevC.94.035804>
- [102] Hinderer T 2008 *Astrophys. J.* **677** 1216–1220
- [103] Hinderer T 2009 *Astrophys. J.* **697** 964
- [104] Hinderer T, Lackey B D, Lang R N and Read J S 2010 *Phys. Rev. D* **81** 123016
- [105] Binnington T and Poisson E 2009 *Phys. Rev. D* **80** 084018

- [106] Damour T and Nagar A 2010 *Phys. Rev. D* **81** 084016
- [107] Stergioulas N and Morsink S *RNS code* URL <http://www.gravity.phys.uwm.edu/rns/>
- [108] Abbott B P *et al.* 2018 arXiv:1805.11579
- [109] Margalit B and Metzger B D 2017 *Astrophys. J.* **850** L19
- [110] Rezzolla L, Most E R and Weih L R 2018 *Astrophys. J.* **852** L25
- [111] Annala E, Gorda T, Kurkela A and Vuorinen A 2018 *Phys. Rev. Lett.* **120** 172703
- [112] Most E R, Weih L R, Rezzolla L and Schaffner-Bielich J 2018 *Phys. Rev. Lett.* **120** 261103
- [113] Lim Y and Holt J W 2018 *Phys. Rev. Lett.* **121** 062701
- [114] Raithel C, Özel F and Psaltis D 2018 *Astrophys. J.* **857** L23
- [115] Bauswein A, Just O, Janka H T and Stergioulas N 2017 *Astrophys. J.* **850** L34
- [116] Fattoyev F J, Piekarewicz J and Horowitz C J 2018 *Phys. Rev. Lett.* **120** 172702
- [117] Abrahamyan S *et al.* 2012 *Phys. Rev. Lett.* **108** 112502
- [118] Pian E *et al.* 2017 *Nature* **551** 67–70
- [119] Coulter D A *et al.* 2017 *Science* **358** 1556
- [120] Cowperthwaite P S *et al.* 2017 *Astrophys. J.* **848** L17
- [121] Nicholl M *et al.* 2017 *Astrophys. J.* **848** L18
- [122] Alexander K D *et al.* 2017 *Astrophys. J.* **848** L21
- [123] Worley A, Krastev P G and Li B A 2008 *Astrophys. J.* **685** 390–399
- [124] Breu C and Rezzolla L 2016 *Mon. Not. Roy. Astron. Soc.* **459** 646–656
- [125] Chakrabarti S, Delsate T, Gürlebeck N and Steinhoff J 2014 *Phys. Rev. Lett.* **112** 201102
- [126] Cipolletta F, Cherubini C, Filippi S, Rueda J A and Ruffini R 2015 *Phys. Rev. D* **92** 023007
- [127] Ryan F D 1995 *Phys. Rev. D* **52** 5707–5718
- [128] Geroch R P 1970 *J. Math. Phys.* **11** 2580–2588
- [129] Hansen R O 1974 *J. Math. Phys.* **15** 46–52
- [130] Pappas G and Apostolatos T A 2012 *Phys. Rev. Lett.* **108** 231104
- [131] Krishnendu N V, Arun K G and Mishra C K 2017 *Physical Review Letters* **119** 091101
- [132] Berti E *et al.* 2015 *Classical and Quantum Gravity* **32** 243001